

# Simple method of detecting ferroelectric domains with non-phase-matched second-harmonic generation

Russell J. Gehr, W. J. Alford, and A. V. Smith

We demonstrate a new method of detecting the presence of ferroelectric domains based on non-phase-matched second-harmonic generation. If a domain boundary is tilted relative to the input and output faces of the crystal, the far-field second-harmonic light consists of multiple beams, in contrast to the single beam generated in a single-domain crystal. The angular separation of the beams provides a measure of the tilt of the domain wall if the refractive-index difference  $n_{2\omega} - n_{\omega}$  is known. © 1998 Optical Society of America

OCIS codes: 190.0190, 190.1900, 190.4400, 160.4330.

## 1. Introduction

Applications of nonlinear optics such as frequency doubling and parametric amplification demand high-quality nonlinear crystals. In an earlier paper<sup>1</sup> we measured parametric gain and phase-matching curves for a number of KTP (KTiOPO<sub>4</sub>) and  $\beta$ -BaB<sub>2</sub>O<sub>4</sub> crystals and found that several of the KTP crystals appeared to have multiple ferroelectric domains with a reversed nonlinear coefficient. Because such 180° domain reversals do not affect a crystal's linear optical properties, testing for reversed domains has relied on piezoelectric<sup>2</sup> or pyroelectric<sup>3,4</sup> probes, x-ray diffraction and topography,<sup>5</sup> chemical etching,<sup>6</sup> electrostatic toning,<sup>2</sup> scanning secondary-electron microscopy,<sup>7</sup> electro-optical techniques,<sup>3</sup> and phase-matched second-harmonic generation<sup>1,8</sup> or non-phase-matched harmonic scattering<sup>9,10</sup> and generation.<sup>11</sup> Only the optical methods provide convenient probes for mapping in detail the domain structure within the crystal. The electro-optic method gives the ratio  $L^+/L^-$ , where  $L^+$  and  $L^-$  are the total line-of-sight lengths with plus and minus ferroelectric polarization. It could in principle be used to map the domain structure tomographically. Phase-matched second-harmonic generation by use of crossed fundamental beams can map the domain

structure, but it requires a specific laser wavelength for each crystal orientation, as well as careful measurements of the phase-matching properties. Our new method is closely related to the second-harmonic scattering method but it is sensitive to large, tilted, planar domain boundaries rather than to the size distribution of multiple small domains. Its advantages are that, with a single pulse from an appropriate *Q*-switched laser, any nonlinear optical crystal can be certified to contain no tilted domain boundaries, or the tilt angle of each boundary can be determined from the angles of second-harmonic beams. No crystal electrodes are needed and the only requirements for the laser are that it be intense enough to produce observable non-phase-matched second harmonic and that its fundamental and harmonic wavelengths lie within the transmission range of the crystal.

## 2. Background

The influence of a tilted, planar domain boundary is perhaps best described in terms of the driven and free harmonic waves that are often invoked in solving Maxwell's equations describing second-harmonic generation,<sup>12</sup> combined with the nonlinear Snell's laws.<sup>13</sup> The driven wave is the specific solution to the second-harmonic wave equation with the second-harmonic polarization term, whereas the free wave is a general solution without the nonlinear harmonic polarization term. Assuming negligible harmonic conversion, the driven and free waves each have a constant amplitude over the full length of a single-domain, transparent crystal. The phase and amplitude of the driven wave are directly tied to those of the fundamental, so its propagation constant is  $2k_{\omega}$

---

The authors are with Department of Lasers, Optics, and Remote Sensing, Sandia National Laboratories, Albuquerque, New Mexico 87185-1423.

Received 6 October 1997; revised manuscript received 2 February 1998.

0003-6935/98/153311-07\$15.00/0

© 1998 Optical Society of America

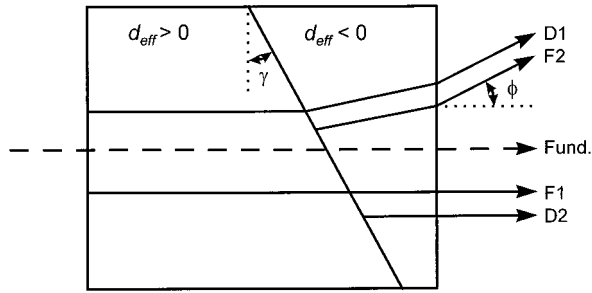


Fig. 1. Diagram of the fundamental wave (dashed line) plus the free (F) and driven (D) second-harmonic waves in a crystal with a tilted planar ferroelectric domain boundary. The sign of the nonlinear coefficient  $d$  is reversed in the two domains. This diagram is for  $\Delta k > 0$ ; for  $\Delta k < 0$ , the deflection is in the opposite direction.

and its amplitude is proportional to  $E_\omega^2 d_{\text{eff}} / \Delta k$ , where  $E_\omega$  is the fundamental field,  $d_{\text{eff}}$  is the effective nonlinear coefficient, and  $\Delta k$  is the phase velocity mismatch  $k_{2\omega} - 2k_\omega$ . At the crystal input face the total harmonic field is zero. At that plane the free wave has a field nearly equal in magnitude to the driven wave but opposite in sign. The free-wave propagation constant is that of a freely propagating harmonic wave  $k_{2\omega}$ , so interference between the free and driven waves creates a harmonic wave with a strength that varies sinusoidally through the crystal according to

$$E_{2\omega}(z) = E_\omega^2 d_{\text{eff}} K z \frac{\sin\left(\frac{\Delta k z}{2}\right)}{\frac{\Delta k z}{2}} \exp(i\Delta k z / 2). \quad (1)$$

If the product of  $\Delta k$  and crystal length  $L$  is varied, by tilting the crystal, for example, this interference is responsible for Maker fringes,<sup>14-16</sup> the sinusoidal variation of output harmonic strength with  $\Delta k L$ .

Assuming low conversion efficiency, ferroelectric domains can be treated as separate crystals each with a driven and free wave, as shown in Fig. 1 for a crystal with two domains separated by a tilted boundary. The four harmonic waves labeled D1, D2, F1, and F2 correspond to the driven (D) and free (F) waves from domains 1 and 2. At the domain boundary, F1 is undeflected because there is no change in the refractive index  $n_{2\omega}$  and consequently no wavelength change. The driven wave from the first domain, D1, becomes a freely propagating wave in the second domain, undergoing a wavelength change at the tilted boundary that is proportional to  $n_{2\omega} - n_\omega$ . To satisfy boundary conditions, it obeys the nonlinear Snell's law,  $n_\omega \sin \alpha = n_{2\omega} \sin \alpha'$ , where  $\alpha$  and  $\alpha'$  are the angles between the propagation direction and the normal to the boundary in the first and second domains, respectively. This confers a tilt on wave D1 upon exiting the second crystal given by

$$\phi = \arcsin \left\{ n_{2\omega} \sin \left[ \gamma - \arcsin \left( \frac{n_\omega}{n_{2\omega}} \sin \gamma \right) \right] \right\}. \quad (2)$$

The exit angle is usually small because the difference in  $n_\omega$ , the refractive index of the fundamental wave, and  $n_{2\omega}$ , the refractive index of the harmonic wave, is small. For small exit angles,  $\phi$  is well approximated by

$$\phi = (n_{2\omega} - n_\omega) \tan \gamma = \frac{\Delta k}{2k_0} \tan \gamma, \quad (3)$$

where  $k_0$  is the wave vector for the fundamental in air.

The requirement that the sum of the free and driven fields of the second domain be zero at the boundary, or entrance face of the second domain, forces F2 to follow the same path as D1. The driven wave from the second domain, with its phase locked to the fundamental, must copropagate with the fundamental. Because of the sign reversal of  $d_{\text{eff}}$  between domains,  $E_{D1}(\text{boundary}) = -E_{D2}(\text{boundary})$ . Combined with the boundary condition for the second domain,  $E_{D2}(\text{boundary}) = -E_{F2}(\text{boundary})$ , we can see that  $E_{F2}(\text{boundary}) = E_{D1}(\text{boundary})$  so waves D1 and F2 constructively interfere at the boundary. Possessing the same propagation vector in the second domain, they continue to constructively interfere outside the crystal. By similar arguments the untilted waves F1 and D2 also constructively interfere at the boundary. However, they have different propagation constants in the second domain and can constructively or destructively interfere outside the crystal, depending on the length of the crystal. In fact, the interference pattern is the same as the Maker fringe pattern for a single-domain crystal of the same total length except they are reversed in phase.

An alternative description of the influence of domains is based on the fact that, for low conversion efficiency, the far-field second-harmonic amplitude is the three-dimensional Fourier transform of the harmonic polarization within the crystal.<sup>10</sup> Ignoring diffraction, the harmonic field at each point on the exit face of the crystal is the one-dimensional Fourier transform of the harmonic polarization along a ray parallel to the propagation direction of the fundamental. This is the sum of two sinc functions,

$$E_{2\omega}(L) = K \left[ L_1 \frac{\sin(\Delta k L_1 / 2)}{\Delta k L_1 / 2} \exp(i\Delta k L_1 / 2 + i\Delta k L_2) - L_2 \frac{\sin(\Delta k L_2 / 2)}{\Delta k L_2 / 2} \exp(i\Delta k L_2 / 2) \right], \quad (4)$$

where  $K$  is a constant,  $L_1$  is the length of the first domain, and  $L_2$  is the length of the second. This can be written in the form

$$E_{2\omega}(L) = \frac{-iK}{\Delta k} \{ [\exp(i\Delta k L) + 1] - 2 \exp(i\Delta k L_2) \}. \quad (5)$$

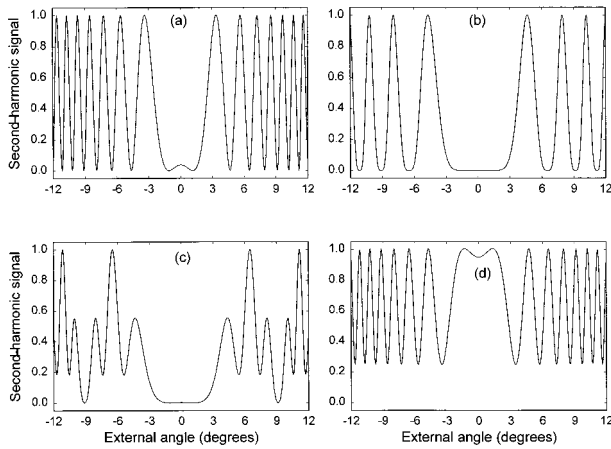


Fig. 2. Simulated Maker fringes for a crystal with (a) a single domain and an untilted boundary separating (b) two equal length domains, (c) two domains with a length ratio of 3:1, and (d) two domains with a length ratio of 200:1.

For a domain boundary tilted by  $\gamma$ , such that  $L_2$  has the form  $L_2(x) = L_0 + x \tan \gamma$ , the harmonic field at the exit face is

$$E_{2\omega}(x) = \frac{iK}{\Delta k} \{ [\exp(i\Delta k L) + 1] - 2 \exp(i\Delta k L_0) \exp(i\Delta k x \tan \gamma) \}. \quad (6)$$

There are two distinct transverse Fourier components; the first, in parentheses, has  $k_x = 0$  and accounts for the forward-going harmonic beam, whereas the second has  $k_x = \Delta k \tan \gamma$ . For small angles, the tilt of this second beam is  $\Delta k \tan \gamma / 2k_0$ , just as in Eq. (3).

For a domain boundary parallel to the crystal faces, there are no tilted beams. All four beams overlap and the Maker fringes can be used to deduce the existence of a domain boundary. More generally, if the coherence length is longer than  $W \tan \gamma$ , where  $W$  is the fundamental beam diameter, the four beams will overlap and interfere. Figure 2 shows some simulated examples with two domains of differing lengths and a domain boundary parallel to the crystal faces. These curves were generated by use of Eq. (4) with  $\Delta k$  and  $L$  dependent on the crystal angle. The details of the simulation are not described here because a marked difference between single-domain [Fig. 2(a)] and two-domain crystals is apparent for any reasonable case. As we noted above, if the boundary is sufficiently tilted that the beams are separated and only the untilted beams are measured, the Maker fringes appear to be those of a single-domain crystal so no domain information is available.

Both the fundamental and the harmonic waves have two eigenpolarizations, identical in the two domains, so there are six possible values of  $\Delta k$  associated with the combinations of fundamental and harmonic polarizations, resulting in as many as six tilted harmonic beams plus six overlapped forward beams. Of course individual processes can often be

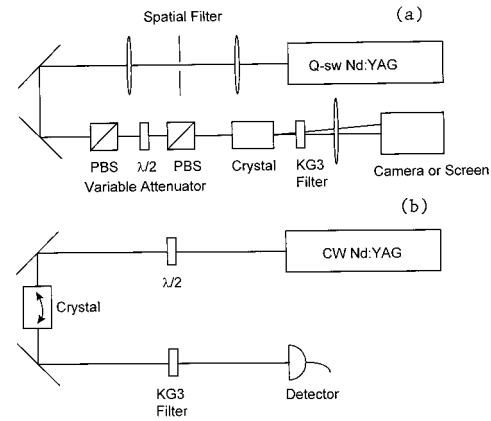


Fig. 3. Experimental setups for (a) non-phase-matched second-harmonic generation and (b) phase-matched second-harmonic generation. PBS, polarizing beam splitter.

isolated by proper choice of the polarization of the input and output light. The tilted beams all lie in the plane defined by the fundamental wave vector  $\mathbf{k}_\omega$  and the normal to the domain boundary. The discussion above applies to each domain boundary, so the pattern of harmonic beams can be complex for multiple boundaries.

### 3. Experimental Methods and Results

Using a *Q*-switched Nd:YAG laser, we examined harmonic beam patterns for a set of eight KTP crystals cut at  $\phi = 0$ ,  $\theta = 58^\circ$  and  $51^\circ$  ( $x$ - $z$  plane), and for several  $x$ -cut KTP and KTA (KTiOAsO<sub>4</sub>) crystals. Four of the critically cut crystals showed clear evidence of domain boundaries. For these we also measured the shape of the second-harmonic phase-matching curves using a 3-W, 1319-nm cw Nd:YAG laser with a beam diameter of 0.5 mm. Our experimental setups are shown in Fig. 3. The 15-ns, 10-mJ, spatially filtered pulses from the *Q*-switched Nd:YAG laser were collimated to a diameter of approximately 1 mm and polarized at  $45^\circ$  with respect to the crystal's  $y$  axis. Each crystal was mounted with the entrance and exit faces perpendicular to the pump beam. The pump light was removed by a KG3 filter after the crystal, and a CCD camera was positioned one focal length away from a focusing lens to obtain the far-field image of the harmonic beams. The focal length of the lens was chosen so that as much of the beam pattern as possible fell on the camera's active area while still maintaining good resolution of the spots. We calibrated beam angles by removing the lens and camera and measuring beam positions on a movable screen for two screen locations separated by approximately 110 cm.

The  $45^\circ$  polarization of the fundamental ensures that the maximum number of nonlinear terms are excited in the angle-cut samples because the fundamental field has components along all three principal axes  $x$ ,  $y$ , and  $z$ . The nonzero coefficients of KTP<sup>17</sup> are  $d_{zyy}$ ,  $d_{yzy}$ ,  $d_{xzx}$ ,  $d_{zxx}$ , and  $d_{zzz}$ . We cannot distinguish between  $x$  and  $z$  polarization with our crystal

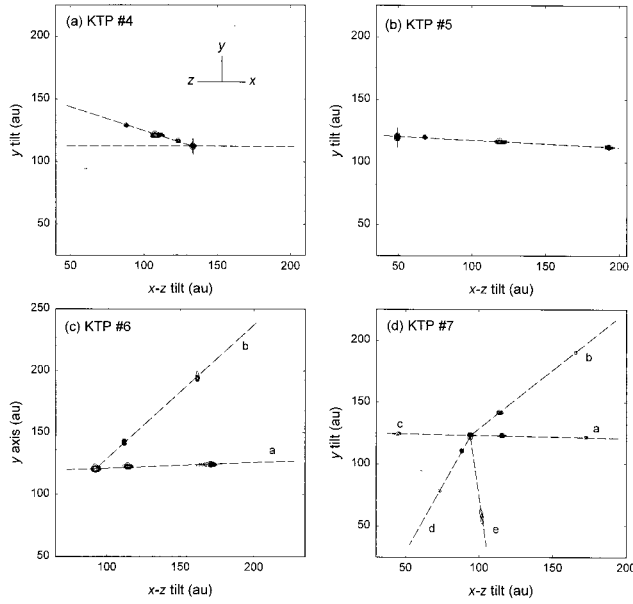


Fig. 4. Beam patterns for the second-harmonic light generated by multiple-domain KTP crystals. (a) Crystal 4, one array of beams indicating a single-domain boundary. (b) Crystal 5, one array of beams believed to be due to two closely spaced parallel domain boundaries. (c) Crystal 6, two arrays of beams indicating two nonparallel domain boundaries. (d) Crystal 7, five arrays of beams indicating five domain boundaries. In (a) and (b), the untilted beam is indicated by the vertical line; in (c) and (d) the untilted beam is at the intersection of the arrays. In (c) and (d) the third beam of each array is outside the camera's field of view.

orientation so the last three  $d$ 's contribute to a single mixing process that we designate  $zzz$ . Using the KTP Sellmeier equation of Vanherzeele *et al.*,<sup>18</sup> we calculate the values of  $\Delta k$ 's corresponding to the three distinct nonlinear processes for doubling 1064-nm light as  $\Delta k_{zyy} = 2k_0(n_{2\omega}^e - n_{\omega}^y) = 2k_0(0.10705)$ ,  $\Delta k_{yzy} = k_0(2n_{2\omega}^y - n_{\omega}^y - n_{\omega}^e) = 2k_0(0.01469)$ ,  $\Delta k_{zzz} = 2k_0(n_{2\omega}^e - n_{\omega}^e) = 2k_0(0.05155)$  for the  $58^\circ$  crystals and  $\Delta k_{zyy} = 2k_0(n_{2\omega}^e - n_{\omega}^y) = 2k_0(0.09428)$ ,  $\Delta k_{yzy} = k_0(2n_{2\omega}^y - n_{\omega}^y - n_{\omega}^e) = 2k_0(0.019984)$ ,  $\Delta k_{zzz} = 2k_0(n_{2\omega}^e - n_{\omega}^e) = 2k_0(0.049367)$  for the  $51^\circ$  crystal. Here  $n^e$  and  $n^y$  are, respectively, the refractive indexes for polarizations in the  $x$ - $z$  plane or normal to it. We expect that the three different values of  $\Delta k$  will lead to three tilted harmonic beams from each domain boundary.

Four of the angle-cut KTP crystals produced multiple beams as shown by the fluence contour plots of Fig. 4. The crystals were oriented so that the birefringent walk-off was to the left, meaning that the projection of the  $x$ ,  $y$ , and  $z$  axes on the crystal input face is that indicated in Fig. 4(a). By use of the same crystal numbers as in our earlier measurements<sup>1</sup> of  $d_{\text{eff}}$ , the multidomain crystals are numbered 4, 5, 6, and 7. Crystal 4 is cut at  $51^\circ$  whereas crystals 5, 6, and 7 are cut at  $58^\circ$ . All four crystals have clear apertures of  $5 \text{ mm} \times 5 \text{ mm}$  and lengths of approximately 10 mm. The corresponding phase-matching curves for second-harmonic generation of 1319-nm light are shown in Fig. 5. In Table 1 we compare the

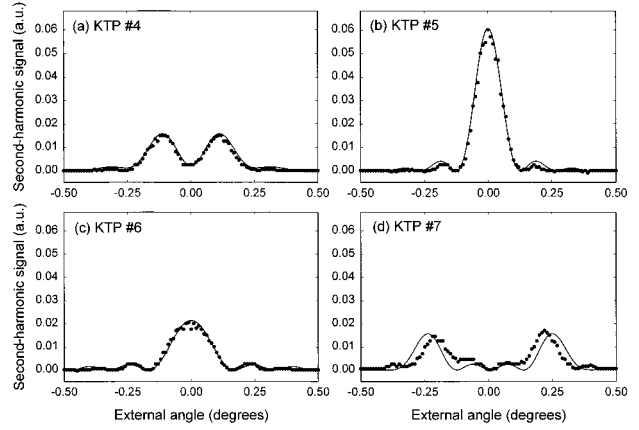


Fig. 5. Measured (filled circles) and simulated (curves) phase-matching curves for second-harmonic generation of  $1.32 \mu\text{m}$  for multiple-domain KTP crystals. (a) Crystal 4, data display two peaks typical of a two-domain crystal. The simulated curve is for two domains with a length ratio of 62.5:37.5. (b) Crystal 5, data appear similar to that for a single-domain crystal, except for slightly larger than usual secondary peaks. The simulated curve is for three domains with a length ratio of 28:1:19. (c) Crystal 6, data show a peak that is significantly broader than for single domain. Simulated curve is for three domains with a length ratio of 3:42:3. (d) Crystal 7, data indicate more than two domains. Simulated curve is for four equal length domains.

measured ratios of beam angles for each domain boundary with the expected ratios based on the  $\Delta k$  values above. The good agreement supports our identification of the origin of the tilted beams. Furthermore, the strengths of the various beams vary as expected with rotation of the polarization of the fundamental and with polarization analysis of the harmonic.

With the fundamental beam centered on crystal 4, the resulting harmonic beam pattern shown in Fig. 4(a) indicates a single-domain boundary orientation, and this is supported by the phase-matching data of Fig. 5(a) which agree well with that expected of two domains with a length ratio of approximately 2:1. However, if the fundamental beam is translated in the  $z$  direction, the harmonic pattern changes to one tilted to the right and slightly up whereas the pattern shown in Fig. 4(a) disappears. The domain boundary appears to consist of two planes that intersect

Table 1. Comparison of Measured ( $\phi$ 's) and Calculated ( $\Delta n$ 's) Second-Harmonic Beam Tilt Ratios

Boundary Number	$\phi_{zzz}/\phi_{yzy}$	$\Delta n_{zzz}/\Delta n_{yzy}$	$\phi_{zyy}/\phi_{yyz}$	$\Delta n_{zyy}/\Delta n_{yyz}$
4a	$2.4 \pm 0.3$	2.47	$4.5 \pm 0.7$	4.72
4b	$2.7 \pm 0.3$	2.47	$5.1 \pm 0.5$	4.72
5	$3.8 \pm 0.3$	3.51	$7.6 \pm 0.7$	7.29
6a	$3.5 \pm 0.3$	3.51		
6b	$3.5 \pm 0.1$	3.51		
7a	$3.6 \pm 0.3$	3.51		
7b	$3.6 \pm 0.2$	3.51		
7d	$3.4 \pm 0.4$	3.51		

just to the left of the crystal center. Near the intersection, the harmonic beams are distorted, indicating that the planes do not meet in a straight line. Apparently there is substantial structure on the submillimeter scale near the intersection.

Our interpretation of the beam pattern of Fig. 4(b) is that crystal 5 has a single tilted domain boundary orientation. However, Fig. 5(b) suggests that if there are two domains, one must be very short compared to the crystal length because the phase-matching curve is nearly identical to that of a single-domain crystal. To reconcile the large boundary tilt with the short length of the inverted domain, we postulate that there is a narrow, tilted domain cutting through the crystal with parallel boundaries. The second boundary will create another pair of driven and free waves, D3 and F3. The four tilted waves will then be the constructively interfering pair (F2, D1) from the first boundary and the constructively interfering pair (F3, D2) from the second. These pairs will be dephased by  $(\pi + T\Delta k)$ , where  $T$  is the domain thickness measured along the beam propagation direction. If  $T$  is much less than a coherence length, the tilted beams destructively interfere, eliminating any tilted beam. A tilted beam is created for larger  $T$ 's unless  $T\Delta k$  is a multiple of  $2\pi$ . The coherence length for the  $zyy$  process is approximately  $5 \mu\text{m}$  so domains thicker than  $1 \mu\text{m}$  should be revealed. The three mixing processes,  $zyy$ ,  $yzy$ , and  $zzz$ , have different coherence lengths so we might expect the interference to affect the beam strengths differently. We do indeed measure relative beam strengths of the three beams from this crystal that are different from the other crystals, providing further evidence of the presence of a thin domain with parallel boundaries.

With the fundamental beam centered on the aperture of crystal 6, we generated the more complicated beam pattern of Fig. 4(c) which implies at least two domain boundary orientations and a minimum of three domains. By rastering the fundamental beam over the crystal aperture, we found regions where only one boundary orientation was evident or where three appeared. Two of the boundaries must intersect each other or the crystal faces. The phase-matching data of Fig. 5(c) are matched well by three domains with a length ratio of 3:42:3.

Crystal 7 created the complex pattern of Fig. 4(d) indicating at least five boundary orientations. One of the boundaries does not traverse the entire crystal. In addition, one of the spots is slightly elongated suggesting that the associated domain boundary is curved or irregular. The phase-matching data of Fig. 5(d) also indicate the existence of several domains. The solid curve, calculated for a crystal with four equal length domains, gives a fair approximation to the data.

The  $x$ -cut crystals generated only one second-harmonic beam, implying that the crystals are either single domain or the domain boundaries are parallel to the crystal faces. We used the Maker fringe method to look for evidence of multiple domains but

found that the fringes were regular and fit accurately those calculated for a single-domain crystal. We conclude that the  $x$ -cut KTP and KTA crystals are all single domain.

#### 4. Identification of Crystal Planes of Domain Boundaries

It is interesting to compare our observed domain boundaries with KTP's crystallographic planes. To calculate the tilts expected of a particular plane identified by the Miller index  $(\ell mn)$ , we construct a unit vector perpendicular to the crystal plane:

$$\hat{d} = \frac{\frac{\ell}{a}\hat{x} + \frac{m}{b}\hat{y} + \frac{n}{c}\hat{z}}{\left[\left(\frac{\ell}{a}\right)^2 + \left(\frac{m}{b}\right)^2 + \left(\frac{n}{c}\right)^2\right]^{1/2}}, \quad (7)$$

another parallel to  $k_\omega$ :

$$\hat{k} = \sin \theta \hat{x} + \cos \theta \hat{z}, \quad (8)$$

and one perpendicular to  $k_\omega$ :

$$\hat{p} = \cos \theta \hat{x} - \sin \theta \hat{z}, \quad (9)$$

where  $\theta$  is the cut angle of the crystal, i.e., the angle between  $k_\omega$  and the  $\hat{z}$  in the  $x$ - $z$  plane, and  $a$ ,  $b$ , and  $c$  are the crystal lattice constants. The angle between  $\hat{k}$  and  $\hat{d}$ , the boundary tilt, is given by

$$\gamma = \arccos(\hat{k} \cdot \hat{d}) = \arccos \left\{ \frac{\frac{\ell}{a} \sin \theta + \frac{n}{c} \cos \theta}{\left[\left(\frac{\ell}{a}\right)^2 + \left(\frac{m}{b}\right)^2 + \left(\frac{n}{c}\right)^2\right]^{1/2}} \right\}, \quad (10)$$

leading to a beam tilt according to Eq. (3) of  $\phi = (n_{2\omega} - n_\omega) \tan \gamma$ . The  $y$  and  $x$ - $z$  components of tilt are

$$\phi_y = \phi \frac{\hat{d} \cdot \hat{y}}{[(\hat{d} \cdot \hat{y})^2 + (\hat{d} \cdot \hat{p})^2]^{1/2}}, \quad (11)$$

$$\phi_{xz} = \phi \frac{\hat{d} \cdot \hat{p}}{[(\hat{d} \cdot \hat{y})^2 + (\hat{d} \cdot \hat{p})^2]^{1/2}}. \quad (12)$$

Using lattice constants<sup>19</sup>  $a = 12.8 \text{ \AA}$ ,  $b = 6.4 \text{ \AA}$ , and  $c = 10.6 \text{ \AA}$ , where  $a$ ,  $b$ , and  $c$  correspond to the optic axes  $x$ ,  $y$ , and  $z$ , respectively, and a crystal cut of  $\theta = 58^\circ$  or  $51^\circ$  in the  $x$ - $z$  plane, we attempted to find the crystallographic planes that give the best match of calculated and measured  $\phi$ 's. For the latter we use the three measured beam angles associated with each domain boundary to find an average value of  $\phi_{yyz}$  according to  $\langle \phi_{yyz} \rangle = (\phi_{yyz} + \phi_{zzz}/3.51 + \phi_{zyz}/7.29)/3$  for the  $58^\circ$  crystal or  $\langle \phi_{yyz} \rangle = (\phi_{yyz} + \phi_{zzz}/2.47 + \phi_{zyz}/4.72)/3$  for the  $51^\circ$  crystal. The results are shown in Fig. 6. Three domain boundaries were found to lie in the  $(100)$  plane perpendicular to the  $x$  axis. The predominance of this plane has been predicted<sup>20</sup> and noted experimentally.<sup>2</sup> However, we also observe two cases of domain boundaries lying in

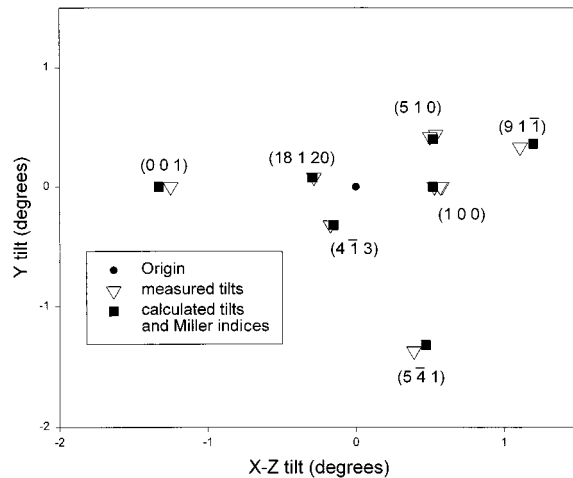


Fig. 6. Measured (open triangles) tilt angles  $\langle\phi_{zxy}\rangle$  and computed tilt angles (filled squares) for best-fit low-order crystallographic planes identified by their Miller indices.

or near the  $(5\ 1\ 0)$  plane plus single examples of boundaries near planes  $(0\ 0\ 1)$ ,  $(4\ \bar{1}\ 3)$ ,  $(5\ \bar{4}\ 1)$ ,  $(9\ 1\ \bar{1})$ , and  $(18\ 1\ 20)$ . A comparison of measured and calculated beam tilts is shown in Table 2.

Whether the domain boundaries are truly planar and lie in crystalline planes is open to question. Our measurements are not precise enough to provide a definitive answer. However, we can report that over our beam diameter of approximately 1 mm the planes are quite flat as indicated by the small angular spread of the tilted harmonic beams. Furthermore, the tilts appear to be quite stable as the fundamental beam is scanned over the crystal aperture, implying that the domain boundary angles are planar over several millimeters. Our measurements could be made much more precise by selecting only the  $zxy$  process that produces the largest tilts and making more precise angle measurements. Alternatively, the fundamental beam diameter could be reduced by at least a factor of 10 without causing an overlap of the tilted and untilted beams that is due to diffraction, so transverse spatial resolution better than 100  $\mu\text{m}$  is possible at the price of reduced angular precision.

Table 2. Comparison of Measured and Calculated Beam Tilts

Boundary Number	Measured		Crystallographic Plane	Calculated $\phi_y, \phi_{xz}$
	$\phi_y \pm 10\%$	$\phi_{xz} \pm 10\%$		
4a	$0.08^\circ, -0.28^\circ$		$(18\ 1\ 20)$	$0.078^\circ, -0.29^\circ$
4b	$0.33^\circ, 1.08^\circ$		$(9\ 1\ \bar{1})$	$0.36^\circ, 1.20^\circ$
5	$0.0^\circ, 0.53^\circ$		$(1\ 0\ 0)$	$0.0^\circ, 0.52^\circ$
6a	$0.0^\circ, 0.58^\circ$		$(1\ 0\ 0)$	$0.0^\circ, 0.52^\circ$
6b	$0.44^\circ, 0.54^\circ$		$(5\ 1\ 0)$	$0.40^\circ, 0.52^\circ$
7a	$0.0^\circ, 0.57^\circ$		$(1\ 0\ 0)$	$0.0^\circ, 0.52^\circ$
7b	$0.42^\circ, 0.50^\circ$		$(5\ 1\ 0)$	$0.40^\circ, 0.52^\circ$
7c	$0.0^\circ, -1.25^\circ$		$(0\ 0\ 1)$	$0.0^\circ, -1.33^\circ$
7d	$-0.32^\circ, -0.17^\circ$		$(4\ \bar{1}\ 3)$	$-0.32^\circ, -0.15^\circ$
7e	$-1.37^\circ, 0.39^\circ$		$(5\ \bar{4}\ 1)$	$-1.32^\circ, 0.47^\circ$

## 5. Conclusions

We have demonstrated a simple, versatile method for detecting tilted domain boundaries in ferroelectric nonlinear crystals that also provides a measure of the domain boundary tilt. Combined with Maker fringe methods, both tilted and untilted domain boundaries can easily be detected with readily available, low-power,  $Q$ -switched Nd:YAG lasers. This technique could provide a convenient method of quality control for ferroelectric nonlinear crystals as well as a useful tool for the study of ferroelectric domain behavior.

This research was supported by the U.S. Department of Energy under contract DE-AC04-94AL85000. Sandia is a multiprogram laboratory operated by Sandia Corporation, a Lockheed Martin company, for the U.S. Department of Energy.

## References

1. D. J. Armstrong, W. J. Alford, T. D. Raymond, and A. V. Smith, "Absolute measurement of the effective nonlinearities of KTP and BBO crystals by optical parametric amplification," *Appl. Opt.* **35**, 2032–2040 (1996).
2. F. Laurell, M. G. Roefols, M. Bindloss, H. Hsuing, A. Suma, and J. D. Bierlein, "Detection of ferroelectric domain reversal in  $\text{KTiOPO}_4$  waveguides," *J. Appl. Phys.* **71**, 4664–4670 (1992).
3. J. D. Bierlein and F. Ahmed, "Observation and poling of ferroelectric domains in  $\text{KTiOPO}_4$ ," *Appl. Phys. Lett.* **51**, 1322–1324 (1987).
4. G. M. Loiacono and R. A. Stolzenberger, "Observation of complex domain walls in  $\text{KTiOPO}_4$ ," *Appl. Phys. Lett.* **53**, 1498–1499 (1988).
5. Z. W. Hu, P. A. Thomas, M. C. Gupta, and W. P. Risk, "Multiple-crystal x-ray topographic characterization of periodically domain-inverted  $\text{KTiOPO}_4$  crystal," *Appl. Phys. Lett.* **66**, 13–15 (1995).
6. M. Houe and P. D. Townsend, "An introduction to methods of periodic poling for second-harmonic generation," *J. Phys. D* **28**, 1747–1763 (1995).
7. G. Rosenman, A. Skliar, I. Lareah, N. Angert, M. Tseitlin, and M. Roth, "Observation of ferroelectric domain structures by secondary-electron microscopy in as-grown  $\text{KTiOPO}_4$  crystals," *Phys. Rev. B* **54**, 6222–6226 (1996).
8. A. Reichert and K. Betzler, "Induced noncollinear frequency-doubling: a new characterization technique for electrooptic crystals," *J. Appl. Phys.* **79**, 2209–2212 (1996).
9. R. S. Cudney, V. Garces-Chavez, and P. Negrete-Regagnon, "Analysis of ferroelectric  $180^\circ$ -domain structures in  $\text{BaTiO}_3$  by use of second-harmonic scattering," *Opt. Lett.* **22**, 439–441 (1997).
10. G. Dolino, "Effects of domain shapes on second-harmonic scattering in triglycine sulfate," *Phys. Rev. B* **6**, 4025–4035 (1972).
11. S. Kurimura and Y. Uesu, "Application of the second harmonic generation microscope to nondestructive observation of periodically poled ferroelectric domains in quasi-phase-matched wavelength converters," *J. Appl. Phys.* **81**, 369–375 (1997).
12. Y. R. Shen, *The Principles of Nonlinear Optics*, (Wiley, New York, 1984).
13. R. L. Sutherland, *Handbook of Nonlinear Optics*, (Marcel Dekker, New York, 1996).
14. J. Jerphagnon and S. K. Kurtz, "Maker fringes: a detailed comparison of theory and experiment for isotropic and uniaxial crystals," *J. Appl. Phys.* **41**, 1667–1681 (1970).

15. W. N. Herman and L. M. Hayden, "Maker fringes revisited: second-harmonic generation from birefringent or absorbing materials," *J. Opt. Soc. Am. B* **12**, 416–427 (1995).
16. D. Chemla and P. Kupecek, "Analyse des experiences de generation de second harmonique," *Rev. Phys. Appl.* **6**, 31–50 (1971).
17. V. G. Dmitriev, G. G. Guradyan, and D. N. Nikogosyan, *Handbook of Nonlinear Optical Crystals*, (Springer-Verlag, New York, 1991).
18. H. Vanherzeele, J. D. Bierlein, and F. C. Zumsteg, "Index of refraction measurements and parametric generation in hydrothermally grown  $\text{KTiOPO}_4$ ," *Appl. Opt.* **27**, 3314–3316 (1988).
19. I. Tardjman, R. Masse, and J. C. Gritel, "Structure cristalline du monophosphate  $\text{KTiPO}_5$ ," *Z. Kristallogr.* **139**, 103–115 (1974).
20. J. D. Bierlein and F. Ahmed, "Observation and poling of ferroelectric domains in  $\text{KTiOPO}_4$ ," *Appl. Phys. Lett.* **51**, 1322–1324 (1987).